

VVAZ analysis of offset VSPs in Altamont-Bluebell field

Khaled Al Dulaijan and Gary F. Margrave

ABSTRACT

The offset VSPs, used for this paper, were acquired within Bluebell Field, the eastern portion of Altamont-Bluebell field in northeastern Utah. Altamont-Bluebell field is within the Uinta Basin, and is considered an unconventional reservoir in the sense that natural fractures act as fluid storage and conduits in the tight sandstones and carbonates. Information related to fracture orientation and intensity is vital for the development of such reservoirs. Azimuthal variations of P-wave velocities can be a valuable tool for fracture information. Therefore, this paper utilizes Velocity Variations with Azimuth (VVAZ) to estimate the direction and intensity of fractured-induced anisotropy within the three main reservoirs using offset VSPs seismic data.

VVAZ inversion method is applied based on the elliptical NMO equation for TI media that was derived by Grechka and Tsvankin (1998). Here, a VVAZ workflow is developed for offset, workaround, or walkaway VSPs using a method for surface seismic. Interval anisotropy properties are calculated for each receiver.

INTRODUCTION

Bluebell-Altamont field is located in northeastern Utah in the Uinta basin. The Uinta basin is an asymmetric east-west trending basin with a south flank that slopes gently. The north flank is bounded by east-west trending Uinta Mountains. The Bluebell-Altamont field is located in the northern-central part of the basin (Figure 1). Production is from Tertiary sandstones, shales and carbonates. There are three main targets in the field: Upper Green River, Lower Green River, and Wasatch/Colton (Lynn et. al, 1995).

The strata were deposited in lacustrine and alluvial environments. The Upper Green River formation was deposited in open-lacustrine and most of the kerogen is immature. Gas may be migrated from deeper formations. The Lower Green River formation was deposited in marginal and open lacustrine. The kerogen-rich shale and marlstone are the sources of oil. Lastly, Wasatch/Colton formation is alluvial and its source of oil is the Kerogen-rich shale. It is a highly overpressured reservoir as a result of hydrocarbon generation. The hydrocarbon generation in the deep Colton formation is the main cause for natural fractures. Natural fractures in the shallower Green River reservoirs are tectonically induced (Morgan et. al., 2003).

Bluebell-Altamont field is unconventional in the sense that natural fractures act as storage and conduits in the tight sandstones and carbonates. Bluebell field is the eastern portion of the Bluebell-Altamont field. Its cumulative production is 336 MMBO, 588 BCFG, and 701 MMBW. The objective of this study is to identify density and direction of fractures to help in determining well spacing to existing wells needed to effectively drain the remaining hydrocarbon reserves in the Bluebell field, and to identify new drilling opportunities (Adams et. al, 2014).

A near offset VSP and 6 offset VSPs are acquired in the field, within the surface seismic survey. The surface seismic is used for VVAZ analysis in another report. To utilize the same method for VSP surveys, a VVAZ workflow is developed in this report for offset, workaround, or walkaway VSPs.

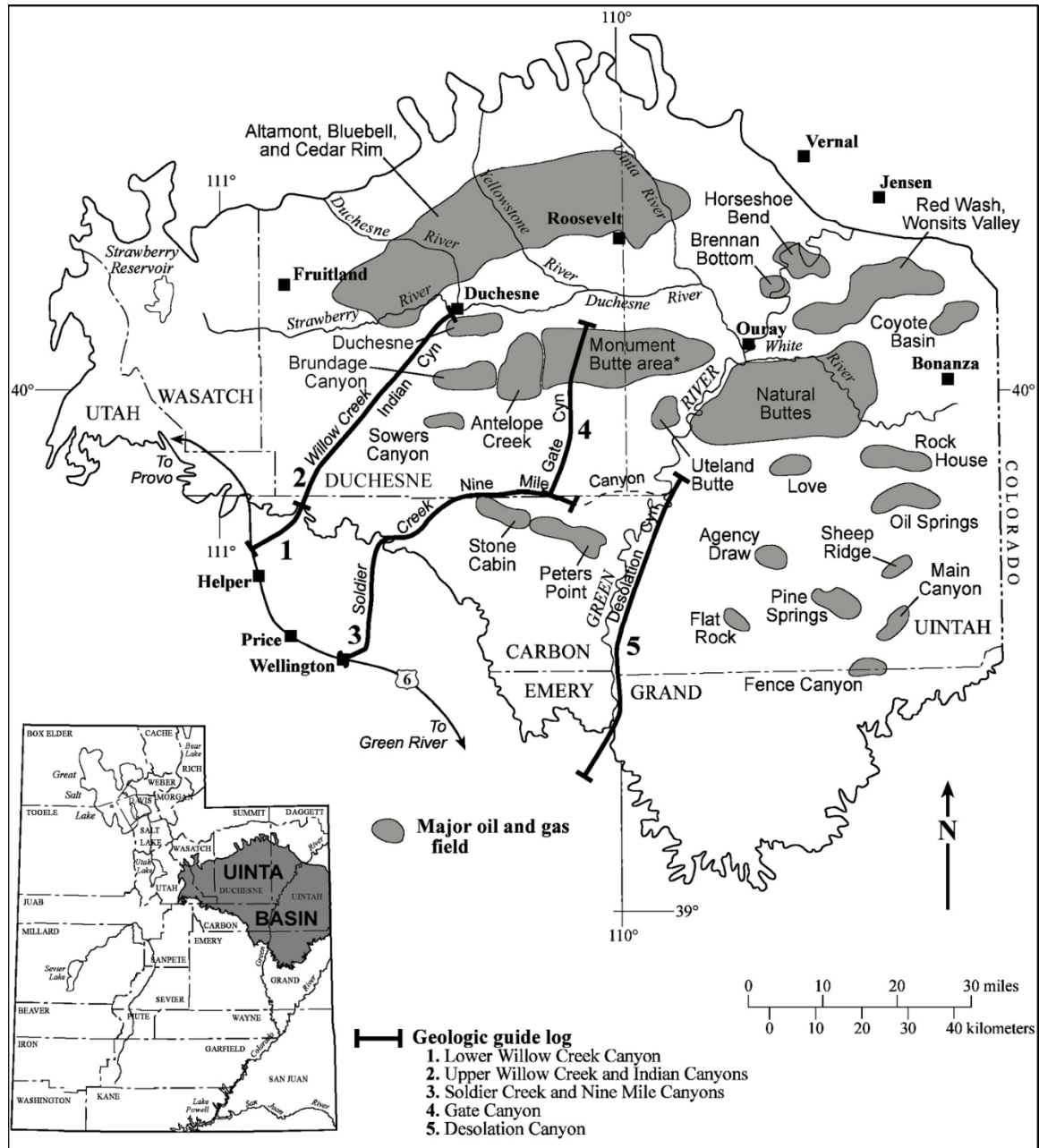


Fig. 1. Location of Uinta basin, Utah (bottom left) and major oil and gas fields within Uinta basin (after Morgan, 2003).

VSP DATA ACQUISITION

A near offset VSP and 6 offset VSPs were acquired using a P-wave source on surface and a 2-level tool of 3-C geophones in the borehole. The natural frequency of the geophones is 15 Hz, and the vibroseis sweep is 4-96 Hz. The total depth (TD) is 14240'. The locations of the sources are shown in Figure 2. The surface elevation of the borehole is 5254' above mean sea level (MSL), while the Kelly Bushing (KB) elevation is 5288' above MSL. Figure 3 shows the acquired depths, offset, and azimuths for each shot. Depths from 8700' to 14000' are covered by 6 shots, and depths above until 3400' were covered by 4 shots. For all depths, one of the shot was a zero-offset VSP.

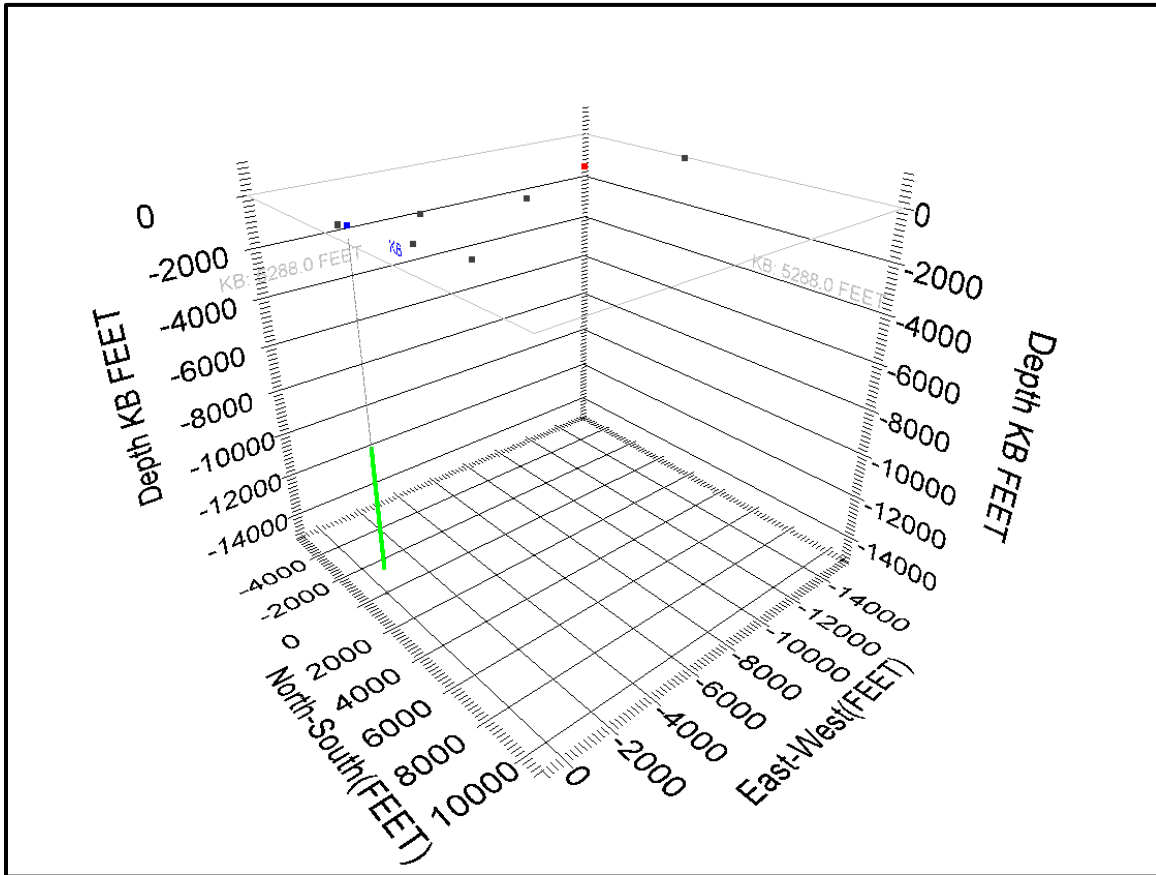


Fig. 2 A schematic diagram showing borehole and downgoing raypath from shot to geophone, indicated by black arrow. **X** is the borehole-shot offset. Vertical raypath from shot elevation is indicated by red arrow. Blue arrow indicates vertical raypath to SRD. The shot to geophone traveltimes is calculated from SDR and indicated by green arrow.

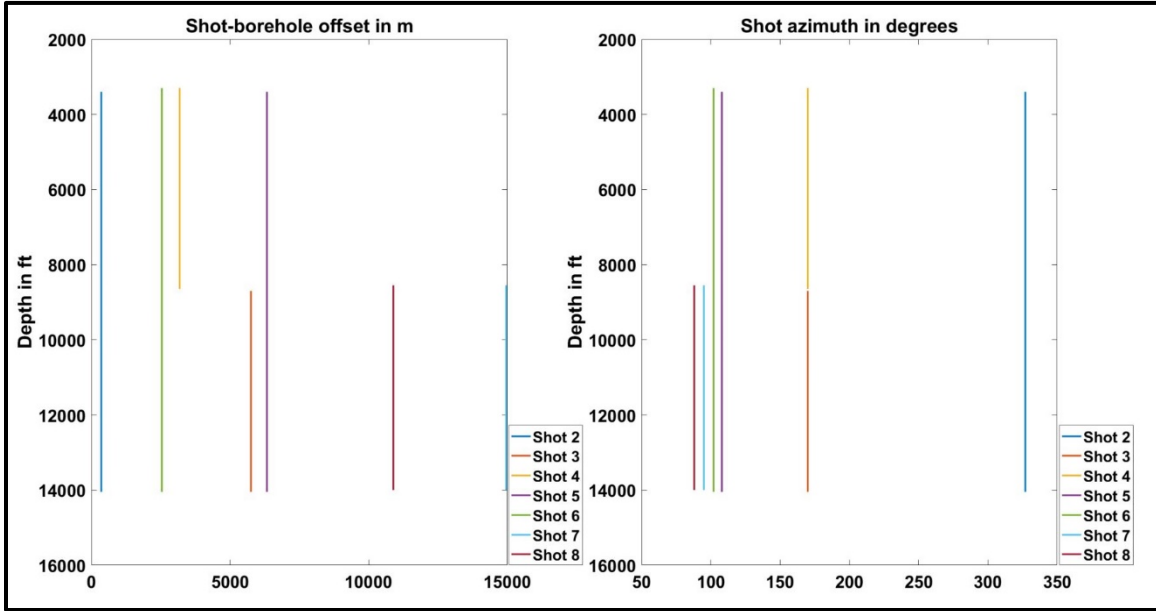


Fig. 3 Acquired depths, offset, and azimuths for each shot.

VSP DATA ANALYSIS

An exponential gain was applied to the data to compensate for spherical divergence. Also, a bandpass filter was applied. First P-wave arrivals were picked for all shots. Figure 4 shows a VSP gather for shot 2 after spherical divergence and bandpass filter. Shot 2 is a near-offset VSP. First P-wave arrivals are indicated by green picks.

Prior to VVAZ analysis. First arrival times were manipulated to reflect surface seismic RMS velocities and to account for the variant surface elevation. A schematic diagram showing the borehole and downgoing raypath from shot to geophone, indicated by black arrow are shown in Figure 5. X is the borehole-shot offset. Vertical raypath from shot elevation is indicated by red arrow. Blue arrow indicates vertical raypath to SRD. The shot to geophone traveltime is calculated from SDR and indicated by green arrow. And finally the traveltime from SRD is doubled, so the geophone can be treated as a CDP in surface seismic geometry. The equations were derived using geometry as below:

$$VT_{SE} = TT_{SE} \cdot \cos(\tan^{-1}[\frac{x}{MD-KB+SE}]), \tag{1}$$

$$VT_{SRD} = VT - \frac{SE-B}{V_{avg}} + \frac{SRD-B}{V_r}, \tag{2}$$

and

$$TT_{SRD} = \frac{VT_{SRD}}{\cos(\tan^{-1}[\frac{x}{MD-KB+SE}])}, \tag{3}$$

where TT_{SE} is first arrival times indicated by the black arrow from shot directly to geophone on Figure 4. VT_{SE} is the vertical time from geophone to shot elevation, and it is indicated by the red arrow. TT_{SRD} is the first arrival time from geophone to shot to Surface Reference Datum (SRD), and it is indicated by the green arrow. MD is the measured depth of geophone from KB. SE is the shot elevation. Finally, B , V_{avg} , and V_r are respectively base of weathering, average velocity, and replacement velocity.

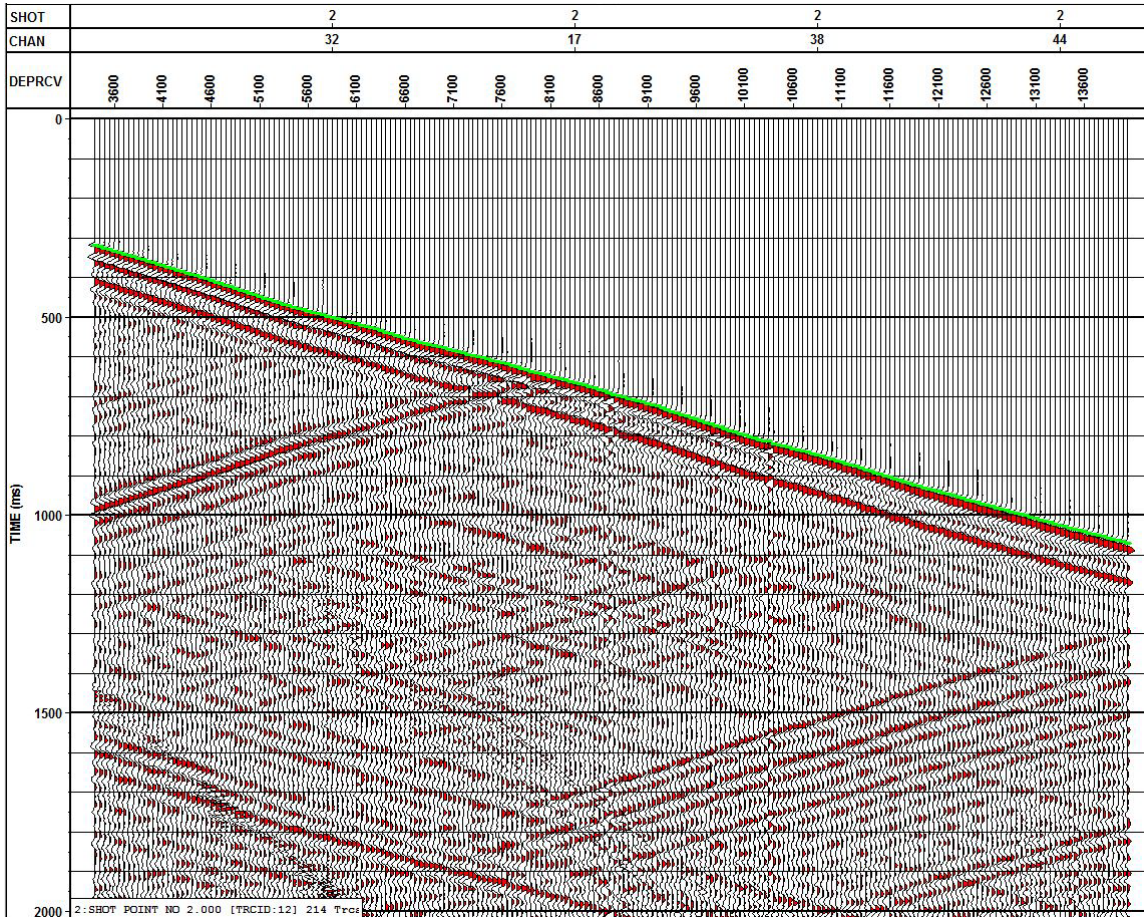


Fig 4. VSP gather for shot 2 after spherical divergence and bandpass filter. Shot 2 is a near-offset VSP. First P-wave arrivals are picked and indicated by green picks.

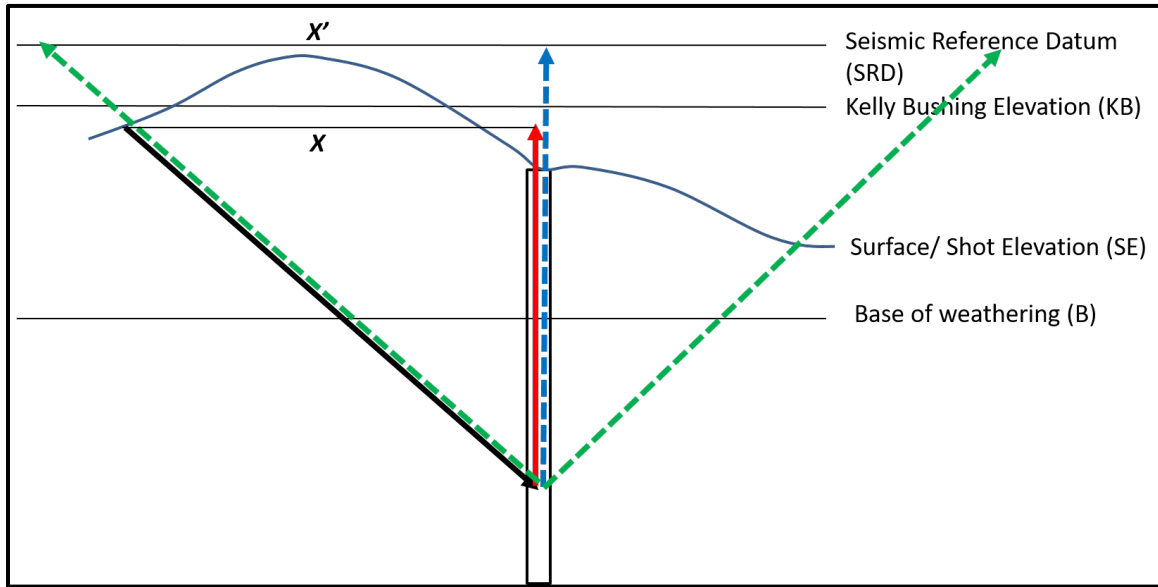


Fig. 5 A schematic diagram showing borehole and downgoing raypath from shot to geophone, indicated by black arrow. X is the borehole-shot offset. Vertical raypath from shot elevation is indicated by red arrow. Blue arrow indicates vertical raypath to SRD. The shot to geophone traveltimes is calculated from SDR and indicated by green arrow.

VELOCITY VARIATIONS WITH AZIMUTH

Grechka and Tsvankin (1998) showed that azimuthal variations of NMO velocities can be estimated by an ellipse in the horizontal plane under four assumption. First, the medium is arbitrarily anisotropic and inhomogeneous, so the azimuthal variations in traveltimes are smooth function of surface locations. Second, traveltimes exist at all azimuth. A case of salt domes creating a shadow zone at a specific azimuth violates the second assumption. Third assumption is routinely assumed in seismic data processing steps, such as CMP binning and stacking. That is traveltimes can be described by a Taylor series expansion of $t^2 x_\phi^2$, where t and x_ϕ are traveltimes and source-receiver offset at specific azimuth. Lastly, traveltimes increase with offset at all azimuths. Those assumptions are nonrestrictive in most cases. Grechka and Tsvankin (1998) derived an elliptical NMO equation for TI media where source-receiver offset do no exceed the depth of the reflector. Hyperbolic NMO can be approximated by:

$$T^2 = T_0^2 + \frac{x^2}{v_{NMO}^2(\phi)} \quad (4)$$

, where

$$\frac{1}{v_{NMO}^2(\phi)} = \frac{1}{v_{slow}^2} \cos^2(\phi - \beta_s) + \frac{1}{v_{fast}^2} \sin^2(\alpha - \beta_s) \quad (5)$$

, where T is the total two-way traveltimes, T_0 is the zero-offset two-way traveltimes. x is the offset, v_{fast} and v_{slow} are the fast and slow NMO velocities respectively. β_s is the

azimuth of the slow NMO velocity, while $V_{NMO}(\phi)$ is the NMO velocity as function of the source-receiver azimuth (Figure 8).

Equation (2) can be written as:

$$\frac{1}{V_{NMO}^2(\phi)} = W_{11} \cos^2(\phi) + 2W_{12} \cos(\phi) \sin(\phi) + W_{22} \sin^2(\phi) \quad (6)$$

, where W_{11} , W_{12} , and W_{22} are the ellipse coefficients that are related to the slow and fast NMO velocities and to the azimuth of the slow NMO velocity by

$$\frac{1}{V_{fast}^2} = \frac{1}{2} [W_{11} + W_{22} - \sqrt{(W_{11} - W_{22})^2 + 4W_{12}^2}] \quad (7)$$

$$\frac{1}{V_{slow}^2} = \frac{1}{2} [W_{11} + W_{22} + \sqrt{(W_{11} - W_{22})^2 + 4W_{12}^2}] \quad (8)$$

$$\beta_s = \tan^{-1} \frac{W_{11} - W_{22} + \sqrt{(W_{11} - W_{22})^2 + 4W_{12}^2}}{2W_{12}} \quad (9)$$

The azimuth of the fast velocity is 90° away from the azimuth of the slow velocities as shown by Figure 8 (Jenner, 2001). The total travel can be written as:

$$T^2 = T_0^2 + x^2 \cos^2(\phi)W_{11} + 2x \cos(\phi)\sin(\phi)W_{12} + x^2 \sin^2(\phi)W_{22}. \quad (10)$$

Equation (7) can be written as:

$$d = Gm,$$

where d is n-dimensional data vector, m is the 6-dimensional model parameter vector, and G is the n-by-4 data kernel as:

$$\begin{pmatrix} T_1^2 \\ T_2^2 \\ \vdots \\ T_n^2 \end{pmatrix} = \begin{pmatrix} 1 & x_1^2 \cos^2(\phi_1) & 2x_1 \cos(\phi_1)\sin(\phi_1) & x_1^2 \sin^2(\phi_1) \\ 1 & x_1^2 \cos^2(\phi_1) & 2x_1 \cos(\phi_1)\sin(\phi_1) & x_1^2 \sin^2(\phi_1) \\ \vdots & \vdots & \vdots & \vdots \\ 1 & x_{n1}^2 \cos^2(\phi_n) & 2x_{n1} \cos(\phi_n)\sin(\phi_n) & x_{n1}^2 \sin^2(\phi_n) \end{pmatrix} \begin{pmatrix} T_0^2 \\ W_{11} \\ W_{12} \\ W_{22} \end{pmatrix}. \quad (11)$$

For Dix-type interval ellipse coefficients, W_i , we use the Grechka et. al., 1999 relation:

$$W^{-1}_l = \frac{T_0(l)W^{-1}(l) - T_0(l-1)W^{-1}(l-1)}{T_0(l) - T_0(l-1)}, \quad (12)$$

where $(l-1)$ is top layer, and (l) is the bottom layer.

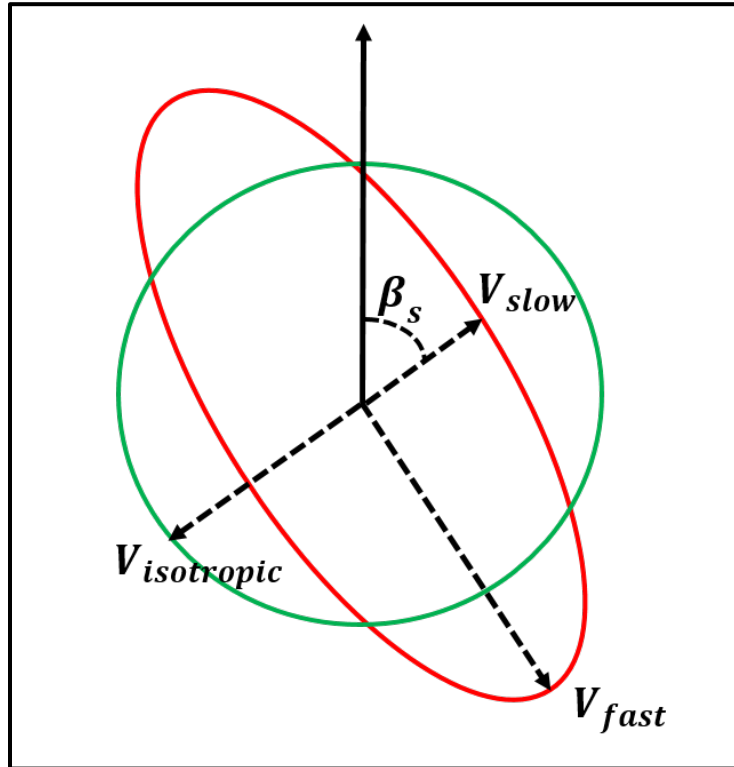


Fig. 6. Isotropic RMS velocity vs azimuthally variant RMS velocity.

RESULTS

For all VSPs, each receiver represents a CDP of conventional surface seismic survey. The corrected arrivaltimes or the double of TT_{SRD} (Equation 3) for all VSPs are used for the VVAZ inversion. Vertical arrivaltimes were inverted and compared to VT_{SRD} in Equation 2 calculated for all VSPs. Inverted arrivaltimes were very close to those of shots 2, 4, and 6 and little off from those of shot 3, 5, 7 and 8, as can be seen in Figure 7. Calculated vertical arrivaltimes of all shots were not very close to each other to start with. Irregular topography and near surface was not corrected precisely. That is the shortcoming of using RMS velocities for VVAZ. A good solution would be using an accurate interval algorithm. Inverted RMS velocities are shown in Figure 8 where the blue curve indicates the fast RMS velocity and the red curve indicates the slow RMS velocity. The orientation of fast RMS velocity for all depths can be seen by the circular histogram in Figure 9. We have estimated Dix-type interval properties of anisotropy in Figure 10. The intervals used to calculate the ellipse coefficients were every receiver (or 50'). On the left is the fast

(blue) and slow (red) interval velocities. On the middle is the anisotropy intensity, and on the right is the interval anisotropy direction.

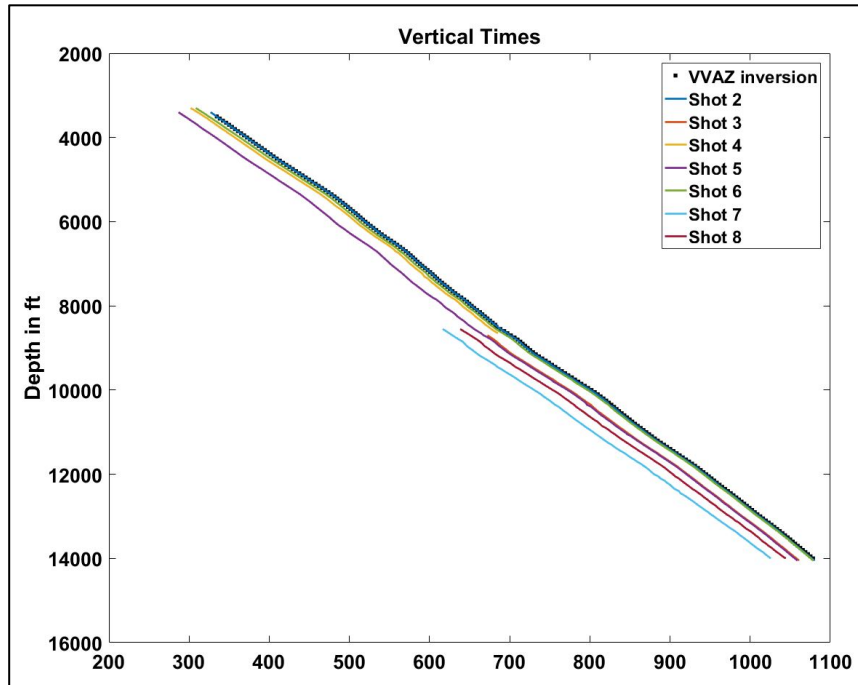


Fig 7. Vertical arrivaltimes of VVAZ inversion vs. calculated vertical traveltimes for each VSP shot.

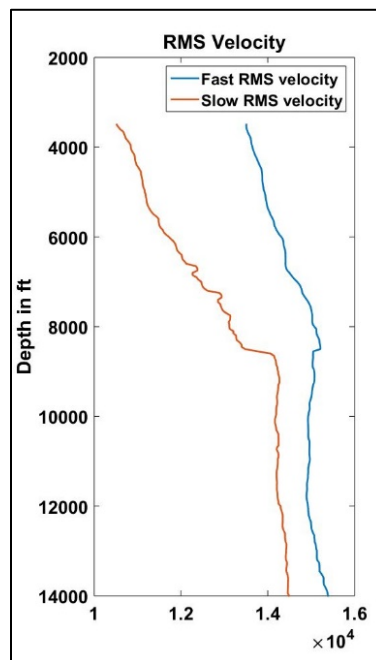


Fig 8. Inverted fast RMS velocity (blue) and slow RMS velocity (red).

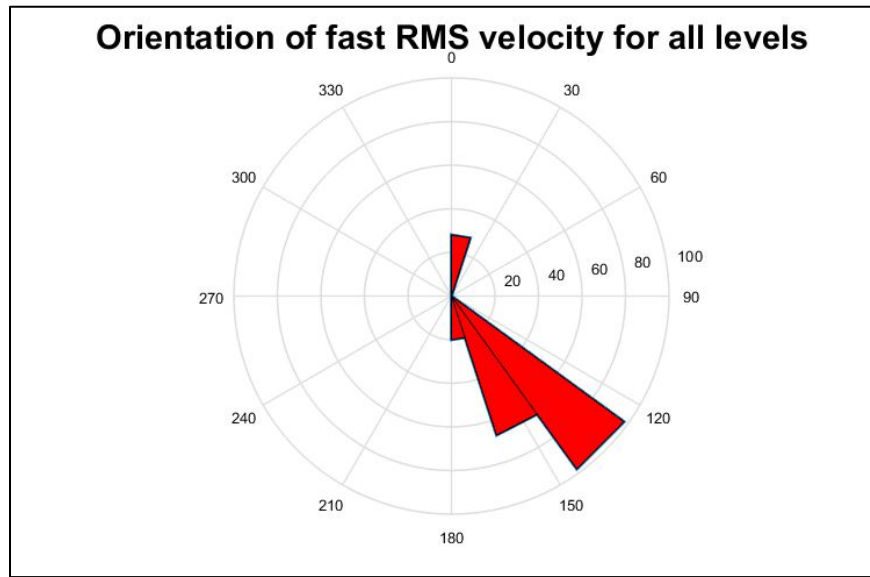


Fig 9. Circular histogram of fast RMS velocity direction for all receivers.

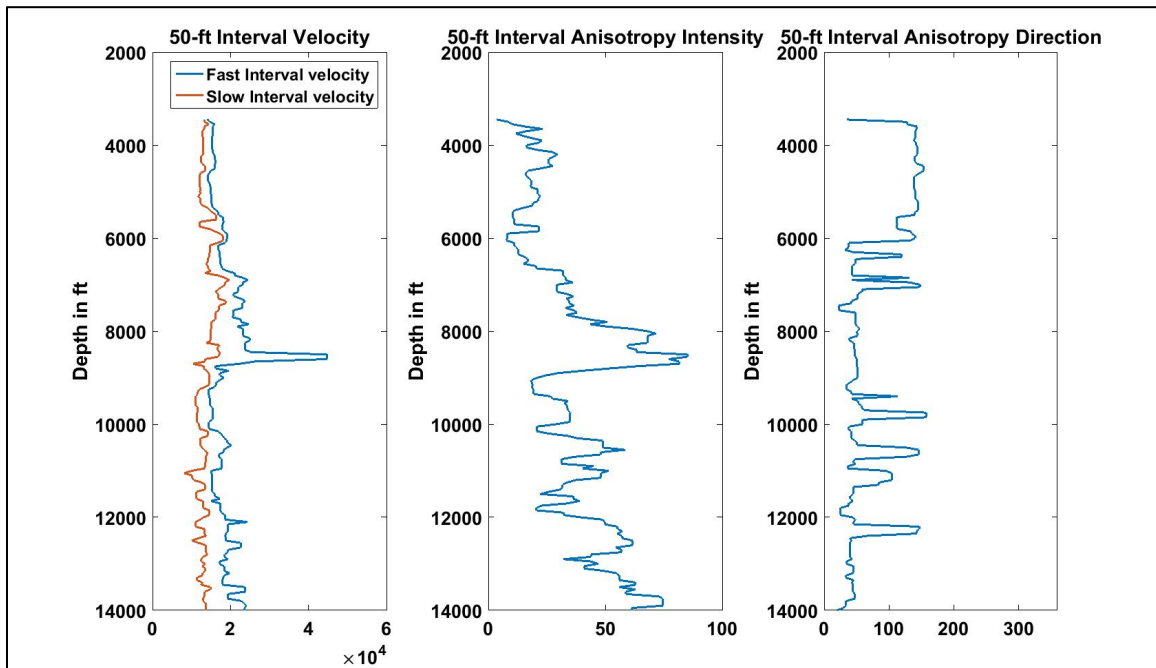


Fig 10. 50'-interval anisotropy: slow and fast RMS velocity (left), anisotropy intensity (middle), and anisotropy direction (right).

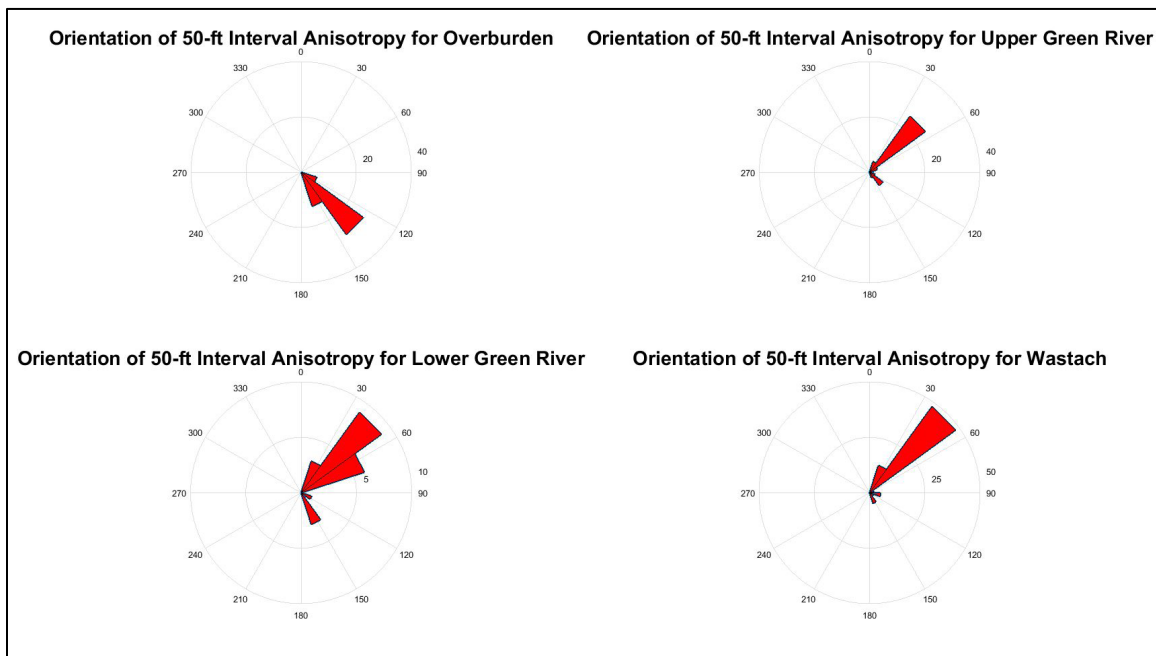


Fig 11. Circular histogram showing the orientation of 50' interval anisotropy of: overburden, Upper Green River, Lower Green River, and Wasatch.

CONCLUSIONS

For the development of unconventional reservoirs, azimuthal variations of P-wave velocities can be a valuable tool for fracture information. In this paper, we have developed a VVAZ workflow for offset, workaround, or walkaway VSPs using a method for surface seismic. Vertical arrivaltimes of all shots were not very close to each other to start with. Irregular topography and near surface was not corrected precisely. That would affect the VVAZ method that is based on RMS velocity here. Therefore, interval anisotropy properties are calculated too to avoid the effects of overburden. The intervals used to calculate the ellipse coefficients were every receiver (or 50').

The three reservoirs were found to have anisotropy oriented at NE-SW trend, while the overburden anisotropy was NW-SE. The anisotropy intensity is found to be highest at the Wasatch formation, and the lower part of the Upper Green River formation.

ACKNOWLEDGEMENTS

We thank the sponsors of CREWES for their support. We also gratefully acknowledge support from NSERC (Natural Science and Engineering Research Council of Canada) through the grant CRDPJ 379744-08. Also, we are grateful to Devon Energy for permission to use the data and publish the results. We thank CGGVeritas for the use of Hampson-Russell software. The first author would like to thank Saudi Aramco for graduate study sponsorship.

REFERENCES

- Adams, C., 2014, Ministry of Natural Gas Development: Northeast BC Activity Update.
- Al Dulaijan, K., G. Margrave and J. Wong, 2015, 3D seismic physical modeling for azimuthal variations of P-wave velocity: CREWES Research Report.
- Al Dulaijan, K., Owusu, J. C., & Weber, D. C., 2012, Azimuthal anisotropy analysis of walkaround vertical seismic profiling vertical seismic profiling: a case study from Saudi Arabia. *Geophysical Prospecting*, 60(6), 1082-1094.
- CGGVeritas, 2014, Hamson-Rusell Software Manual: Release 9.
- Grechka, V., & Tsvankin, I., 1998, 3-D description of normal moveout in anisotropic inhomogeneous media. *Geophysics*, 63(3), 1079-1092.
- Jenner, E., 2001, Azimuthal anisotropy of 3-D compressional wave seismic data, Weyburn Field, Saskatchewan, Canada: Ph.D. thesis, Colorado School of Mines.
- Lucas, P. T., & Drexler, J. M., 1976, Altamont-Bluebell--a major, naturally fractured stratigraphic trap, Uinta basin, Utah.
- Lynn, H. B., Bates, R., Layman, M., & Jones, M., 1995, Natural fracture characterization using P-wave reflection seismic data, VSP, borehole imaging logs, and the in-situ stress field determination. In *Low Permeability Reservoirs Symposium*. Society of Petroleum Engineers.
- Morgan, C. D., 2003, *Geologic Guide and Road Logs of the Willow Creek, Indian, Soldier Creek, Nine Mile, Gate, and Desolation Canyons, Uinta Basin, Utah (OFR-407)*.
- Rüger, A., 2001, Reflection coefficients and azimuthal AVO analysis in anisotropic media. *Society of Exploration Geophysicists*.